Hydrogen Adsorption on Pd–In Intermetallic Surfaces

Topics in Catalysis
https://doi.org/10.1007/s11244-022-01748-6

ORIGINAL PAPER

Hydrogen Adsorption on Pd–In Intermetallic Surfaces

Minttu Kauppinen[1] · **Henrik Grönbeck**[1]

Accepted: 9 November 2022

Abstract
It has recently been shown that CO_2 hydrogenation to methanol over PdIn and In_2O_3 depends critically on the adsorption energy of hydrogen. Here we use density functional theory calculations to investigate hydrogen adsorption over Pd–In intermetallic compound surfaces with different Pd:In ratios. The electronic structure and properties of hydrogen adsorption are investigated for a range of surface facets and compared to the corresponding results for the pure parent metals and Cu. Increased In content is found to shift the Pd(*d*) density of states away from the Fermi level, making the intermetallic Pd–In compounds to appear "Cu-like". We find a linear correlation between the hydrogen binding energy and the *d*-band center of surface Pd atoms. Understanding of how the hydrogen adsorption energy depends on composition and structure provides a possibility to enhance the performance of CO_2 hydrogenation catalysts to methanol.

Keywords Methanol synthesis · Hydrogen activation · Intermetallic · Density functional theory

1 Introduction

CO_2 hydrogenation to methanol is an important reaction towards a closed carbon cycle [1–3]. In_2O_3-based catalysts have shown promising properties for CO_2 hydrogenation with high selectivity and catalyst stability [4–7]. Moreover, the performance has been measured to be further enhanced by promoting In_2O_3 with Pd [5–9]. However, it is not clear what the state of the Pd/In_2O_3 catalyst is and one suggestion is that a PdIn intermetallic compound is formed during reducing conditions [6, 8]. Intermetallic compounds of palladium and indium in the absence of the In_2O_3 oxide have proven to be promising materials for CO_2 hydrogenation to methanol [8], as well as its reverse reaction being methanol steam reforming [10]. The formation of Pd–In intermetallic phases is energetically favourable with respect to the parent metals across the entire composition range, and can be achieved at mild temperatures via reactive metal support interaction (RMSI) by reducing Pd/PdO particles supported on In_2O_3 with hydrogen [6, 10–12].

Alloy formation leads to changes in the geometric and electronic structure of the metal, which has consequences for adsorbate binding and reactivity [13, 14]. In particular, changes in the position of the *d*-band center [15–18] of transition metals upon alloying with another metal can modify the adsorption properties of atoms and molecules. However, adsorption on metal/alloy surfaces does not always follow the simple *d*-band model, and additional descriptors such as *d*-band shape and site coordination have been included to accurately describe adsorption energies [19–21]. A previous computational study shows that the shift in calculated adsorption energies of propane dehydrogenation intermediates correlates with a negative shift in the *d*-band center of Pd-M intermetallic surfaces, with respect to pure Pd [22]. In addition to electronic effects, alloying changes the site assembly at the metal surface. Changes in the site assembly could be important as isolation of the active metal sites could enhance the selectivity of hydrogenation/dehydrogenation reactions [22–24].

In our previous density functional theory (DFT) and microkinetic modelling studies on methanol synthesis over PdIn and In_2O_3, we found that increasing hydrogen stability while keeping other parameters unchanged leads to considerable enhancement of the methanol synthesis rate [25, 26]. Due to the high vapour pressure of In and the complex

✉ Minttu Kauppinen
minttum@chalmers.se

Henrik Grönbeck
ghj@chalmers.se

[1] Department of Physics and Competence Centre for Catalysis, Chalmers University of Technology, 412 976 Göteborg, Sweden

Published online: 19 November 2022

phase-diagram of Pd–In, controlling and predicting the composition of Pd–In intermetallic compounds is generally challenging [24]. Thus, it is important to consider multiple compositions when investigating the effects of alloying on the catalytic properties.

Herein, we have investigated the effect of alloying on the electronic structure and the consequences for hydrogen adsorption properties of Pd–In. Atomic ratios of 1:1, 2:1, and 2:3 (Pd:In) were considered and compared to the single metallic Pd, In, and Cu by employing DFT calculations. The results for PdIn are compared to Cu as Pd–In has been referred to as having a "Cu-like" electronic structure [27–29]. Our results show that alloying Pd with In narrows the *d*-band and shifts the *d*-band center of Pd to a lower energy. The shift to lower energies results in weaker bonding of hydrogen to the surface Pd atoms due to presence of occupied anti-bonding states. The hydrogen adsorption energy is found to correlate with the position of the *d*-band center, providing a convenient descriptor for hydrogen adsorption on Pd–In systems.

2 Computational Methods

The Vienna Ab initio Simulation Package (VASP; version 5.4.4)) was used for the electronic structure calculations [30–34]. The BEEF-vdW [35] functional was used to include dispersion forces. The metal bulk structures were optimised using a 600 eV energy cut-off and a $16 \times 16 \times 16$ /$16 \times 16 \times 12$/$12 \times 12 \times 12$ Monkorst–Pack mesh for (Cu, In, Pd, PdIn)/Pd_2In/Pd_2In_3. Hydrogen, palladium, indium, and copper were treated with 1, 10, 13, and 11 valence electrons, respectively. Table 1 contains a summary of the used bulk structures, as well as the optimised lattice constants with a comparison to experimental data. Our computed lattice constants are slightly elongated compared to the experimental values, in line with previous results for fcc-transition metals using BEEF-vdW [36], however the general agreement is good.

Surface slabs of Pd(111), In(101), Cu(111), PdIn(100),PdIn(110), PdIn(111), PdIn(211), PdIn(310),Pd_2In(100), Pd_2In(110), Pd_2In_3(100), and Pd_2In_3(110) were cut from the bulk structures to represent the most stable single metal surfaces, and multiple Pd–In intermetallic surfaces. The dimensions of the slabs were chosen to achieve approximately the same low hydrogen coverage for all surfaces, and to have a thickness of at least four stoichiometric layers. An energy cutoff of 450 eV and a $3 \times 3 \times 1$ Monkorst–Pack mesh was used for all surface calculations. A 12 Å vacuum was kept between the periodic images of the slabs in the direction perpendicular to the surface. Atoms in the first two stoichiometric layers of the slabs were allowed to relax whereas the rest were fixed at their ideal bulk positions.

Surface formation energies γ of the slabs were calculated as

$$\gamma = \frac{1}{2A}(E_{slab} - NE_{bulk}) \quad (1)$$

where A, E_{slab}, and N are the surface area, total energy, and number of atoms of the slab, respectively. E_{bulk} is the bulk energy per atom. PdIn(100) and PdIn(111) can have either Pd or In terminating the surface. To determine surface energy with respect to the PdIn bulk, the ratio of In and Pd atoms must be the same as in the bulk, but for the PdIn(100) and PdIn(111) surfaces this is only possible if one side of the slab is In terminated, and the other is Pd terminated. Therefore, the surface energy calculated according to Eq. 1 represents the average surface formation energy of both terminations. Furthermore, the In and Pd terminated surfaces can undergo different degrees of relaxation upon surface formation. To account for this, we have used thicker 10/8 stoichiometric layer slabs with the 6/4 middle layers kept fixed to allow the relaxation of both terminations of the (111)/(100) surface slabs.

The hydrogen adsorption energy, ΔE_{ads}, was calculated as

$$\Delta E_{ads} = E_{slab+H} - E_{slab} - 0.5E_{H_2} \quad (2)$$

where E_{slab} and E_{slab+H} are the total energies of the clean slab and a slab with one adsorbed hydrogen atom, respectively. E_{H_2} is the energy of a hydrogen molecule in the gas-phase. ΔE_{ads} is calculated with one H in the surface cell, which is

Table 1 Bulk structures and the corresponding calculated and experimental lattice constants in Å

	Crystal structure	Calc. lattice constants	Exp. lattice constants
In	Body-centered tetragonal	$a = 3.24, c = 4.98$	$a = 3.26, c = 4.94$ [37]
Pd	Face-centered cubic	$a = 3.98$	$a = 3.89$ [38]
PdIn	Primitive cubic	$a = 3.33$	$a = 3.24$ [39]
Pd_2In	Orthorhombic	$a = 4.21, b = 5.61,$ $c = 8.26$	$a = 4.22, b = 5.62,$ $c = 8.23$ [40]
Pd_2In_3	Trigonal	$a = 4.53, b = 5.50$	$a = 4.54, b = 5.51$ [41]
Cu	Face-centered cubic	$a = 3.66$	$a = 3.62$ [42]

appropriate as the systems are metallic, and the H-H interactions are weak [43]. The hydrogen binding energy, E_b, was calculated as

$$E_b = E_{slab+H} - E_{slab} - E_H \quad (3)$$

where E_H is the energy of a hydrogen atom in the gas-phase. For both the adsorption and binding energy, a negative value indicates exothermic adsorption. The geometric relaxation of the hydrogen molecule and single-point calculation of the hydrogen atom were performed in 15 × 15 × 15 Å computational cells.

3 Results and Discussion

3.1 Effect of Alloying Pd with In on the Electronic Structure

The computed density of states (DOS) for the optimised bulk structures (Fig. 1) clearly demonstrate the dramatic effect on the electronic structure of Pd when alloying with In. Upon alloying with In, the Pd *d*-band shifts away from the Fermi energy, appearing more similar to the *d*-band of copper. Furthermore, the magnitude of the *d*-band center shift increases with increasing In content. Although the DOS at Fermi level is drastically reduced, there is no band-gap formation, showing that the Pd–In intermetallic compounds retain metallic character.

To further investigate the electronic structure of the Pd–In compounds, a Bader charge analysis (as implemented by the Henkelman group [44–47]) was conducted. The computed Bader charges (Table 2) clearly show charge transfer from

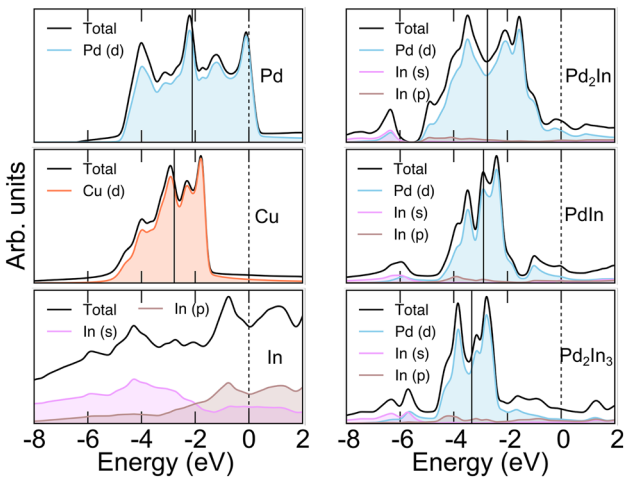

Fig. 1 Density of states for metals and alloy bulk structures. The Fermi energy is shifted to 0 eV and indicated with a dashed vertical line. The *d*-band center is indicated with a solid black line

Table 2 Average bader charges (b.c.) on the Pd and In atoms in Pd–In intermetallic bulks expressed as a change in number of Bader electrons compared to the neutral metal atoms

Bulk	b.c. on Pd	b.c. on In
Pd_2In	− 0.36	+ 0.72
PdIn	− 0.53	+ 0.53
Pd_2In_3	− 0.70	+ 0.47

the less electronegative In to the more electronegative Pd. As the fraction of In atoms in the bulk increases, more charge is transferred to the Pd atoms on average, yet the positive charge per In atom is smaller for the In richer compounds. The Bader charge of ±0.53 obtained for PdIn is in agreement with a previously reported value [24]. The charge transfer to Pd is consistent with the filling of the Pd(*d*) states as shown in the DOS analysis.

The calculated shift of the Pd(*d*) DOS away from the Fermi level is in agreement with previous experimental observations of the valence band spectra of PdIn [8, 27], and DFT calculated DOS of the PdIn bulk [24, 28], and the PdIn(110) surface [28]. Gradually more negative shift upon increased In content is consistent with a previous experimental study, where the shifts were observed in the valence band spectra of Pd–In nanoparticles [8]. A similar decrease in the DOS near the Fermi level has also been previously reported for PdCd and PdZn [48], and Pd-Ga intermetallic compounds [23].

3.2 Surface Energies

Computed surface formation energies γ (Table 3) of the pure metals Pd, In, and Cu are underestimated with respect to experiment, which is a known issue with the BEEF-vdW functional [36]. However, the surface energy of the metals obeys the correct trend that In has the lowest surface energy, and Pd the highest [49]. For PdIn, the surfaces with a higher density of surface atoms and more Pd–In bonds in the first surface layer are more stable than surfaces with lower atom density and more bonds between like atoms. The (100) and (111) facets of PdIn can have a In or Pd surface termination, and for both facets the Pd terminated surface compresses more upon relaxation than the In terminated counterpart. The distance between the top most layer and the first subsurface layer is 1.41/0.36 Å for Pd terminated (100)/(111) surface, whereas the corresponding value on the In terminated (100)/(111) surface is 1.86/1.18 Å. Similar trends with substantial relaxations of Pd atoms have been reported for the PdIn(110) surface, and can be rationalised as Pd has a higher surface energy than In [28].

3.3 Hydrogen Adsorption

Hydrogen adsorption sites were screened by placing a hydrogen atom in each unique bridge, hollow, or top

Table 3 Surface formation energies γ (in meV/Å^2), hydrogen adsorption and binding energies (per atom in eV), and Bader charges on In,Pd,Pd_xIn_y alloy, and Cu surfaces

	Surface	γ	ΔE_{ads}	E_b	b.c. on Pd	b.c. on H
In	(101)	19.6	0.61	− 1.81	–	–
Pd	(111)	84.9	−0.38	− 2.80	+0.02	−0.12
PdIn	(110)	49.9	0.32	− 2.09	−0.41	−0.19
	(211)	58.3	0.25	− 2.16	−0.39	−0.28
	(310)	67.4	−0.02	− 2.43	−0.31	−0.18
	(100),In-t*	70.4	0.28	− 2.14	–	–
	(100),Pd-t*	70.4	0.01	− 2.41	−0.28	−0.16
	(111),In-t*	76.6	0.30	− 2.11	−0.50	−0.24
	(111),Pd-t*	76.6	0.45	− 1.97	−0.35	−0.16
Pd_2In	(100)	65.4	− 0.01	− 2.43	−0.25	−0.18
	(110)	68.6	− 0.02	− 2.44	− 0.25	−0.17
Pd_2In_3	(100)	42.5	0.25	− 2.17	− 0.48	− 0.19
	(110)	45.8	0.25	− 2.17	− 0.53	− 0.19
Cu	(111)	79.2	0.00	− 2.41	–	–

*The tabulated value represents an average surface formation energy of the In and Pd-terminated surfaces of these facets. Bader charges (b.c.) on the Pd and H atoms of H/M adsorption structures are expressed as a change in number of Bader electrons compared to the neutral atoms. The Pd atom Bader charges are indicated for the surface Pd atoms directly bonded to hydrogen upon adsorption, and in cases where more than one Pd atom is involved, it is the average value of those atoms

site on all surfaces and optimising the geometry of each obtained structure. The most favourable hydrogen adsorption geometries on the studied metal and alloy surfaces are presented in Fig. 2, and the corresponding adsorption and binding energies are reported in Table 3. In all cases where hydrogen was placed initially at a Pd top site, the hydrogen atom migrates during the structure relaxation to a nearby bridge or hollow position, i.e. hydrogen adsorbed atop Pd appears not to be a local minima. Hydrogen has the highest binding energy on the un-alloyed Pd(111) surface, where it binds to the fcc hollow site with a binding energy of −2.80 eV. The calculated binding energies for the fcc hollow sites on Pd(111) and Cu(111) agree well with previously computed values [50, 51].

The Pd-Pd bridge site is the preferred adsorption site on all intermetallic surfaces, provided that such a site is present. On the pure In(101) hydrogen binds preferably at the atop site, and the resulting adsorption energy is strongly endothermic. PdIn(310), Pd_2In(100), and Pd_2In(100) have the highest binding energies of the intermetallic surfaces. Interestingly, the weakest adsorption for Pd–In intermetallics is found on the Pd terminated PdIn(111), even though the hydrogen is adsorbed on a Pd-Pd bridge site. The reason for this behaviour could be that one of the Pd atoms involved in the bonding is in the subsurface, which means that it is highly coordinated. The effective coordination of the subsurface Pd atom is higher on Pd terminated PdIn(111) than on the Pd_2In_3(100), where hydrogen also binds to a subsurface Pd atom.

3.4 Electronic Structure Analysis

The antibonding metal-hydrogen states are occupied for hydrogen adsorbed on noble metals, which results in lower hydrogen binding energies. As discussed in the previous section, alloying of Pd with In shifts DOS away from the Fermi level, which results in the antibonding adsorbate states to be occupied, unlike for pure Pd. This is illustrated in the projected density of states (PDOS) on the adsorbed hydrogen and the surface metal atoms (Fig. 3). Another prominent feature in the PDOS, are the H(*s*) and metal *d* resonant states below − 5 eV (w.r.t Fermi level), and Pd–In surfaces which bind hydrogen the strongest also exhibit more localised resonance peaks.

The analysis of the hydrogen binding energy as a function of the *d*-band center shows a linear trend with a small mean absolute error of 0.06 eV and a maximum error of 0.15 eV, i.e. hydrogen binding on Pd–In intermetallic surfaces can be adequately described by the *d*-band model (Fig. 4).

Bader charges on the H atoms and Pd atoms participating in bonding on the Pd and Pd–In surfaces (Table 3) show that hydrogen adsorbs as a negatively charged hydride species. In general, the Pd atoms directly bonded to the adsorbed hydrogen have lower Bader charges compared to the bulk Pd–In values. On the PdIn(211) and In terminated PdIn(111) surfaces where hydrogen adsorbs on a In-Pd bridge site, the hydrogen atoms have the most negative Bader charges. The changes in the PDOS and Bader charges of Pd atoms in the Pd–In intermetallics together indicate that the electronic

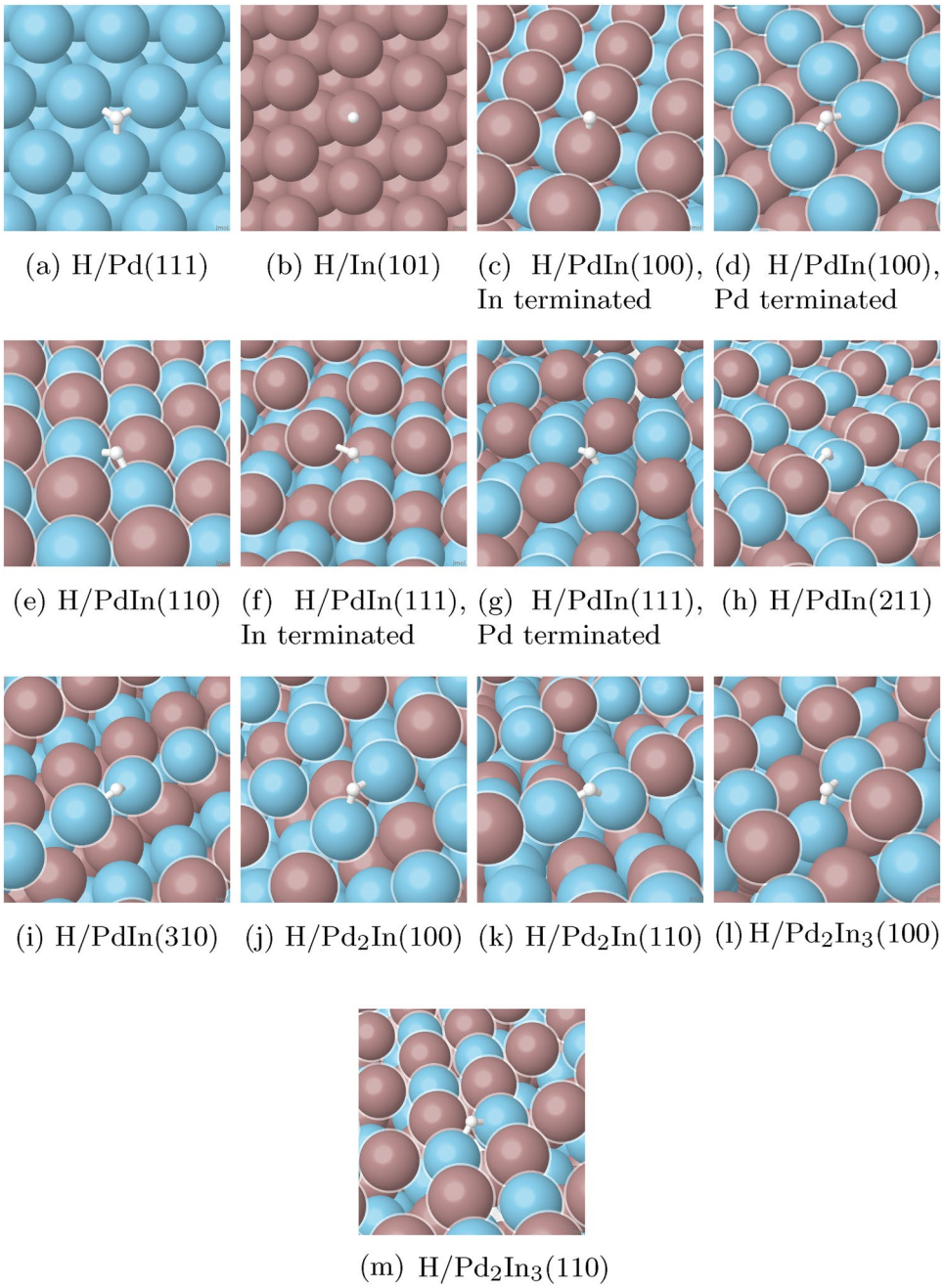

Fig. 2 Most stable hydrogen adsorption structures on Pd, In, and Pd–In alloy surfaces. Pd, In, and H atoms are coloured blue,brown, and white, respectively

configuration is changing from d^9s^1 of elemental (condensed) Pd closer to $d^{10}s^1$, i.e. more similar to the configuration of Cu.

4 Conclusions

Our DFT calculations show that alloying Pd with In causes changes in the electronic structure, shifting the *d*-band center to lower energies further away from Fermi level, making the intermetallic appear more "noble" or "Cu-like". Furthermore, the Bader charge and PDOS analysis together show that the electronic configuration of Pd changes from d^9s^1 to the direction of $d^{10}s^1$ upon alloying with In. Forming the intermetallic compound is also accompanied by charge separation so that the Pd(In) atoms have slightly negative(positive) Pd(In) Bader charges. The systems are, however, still metallic without a band gap. Hydrogen adsorbs as a slightly negatively charged hydride species, and prefers to bind to Pd-Pd bridge sites on all Pd–In intermetallic surfaces, provided that such sites are available, followed

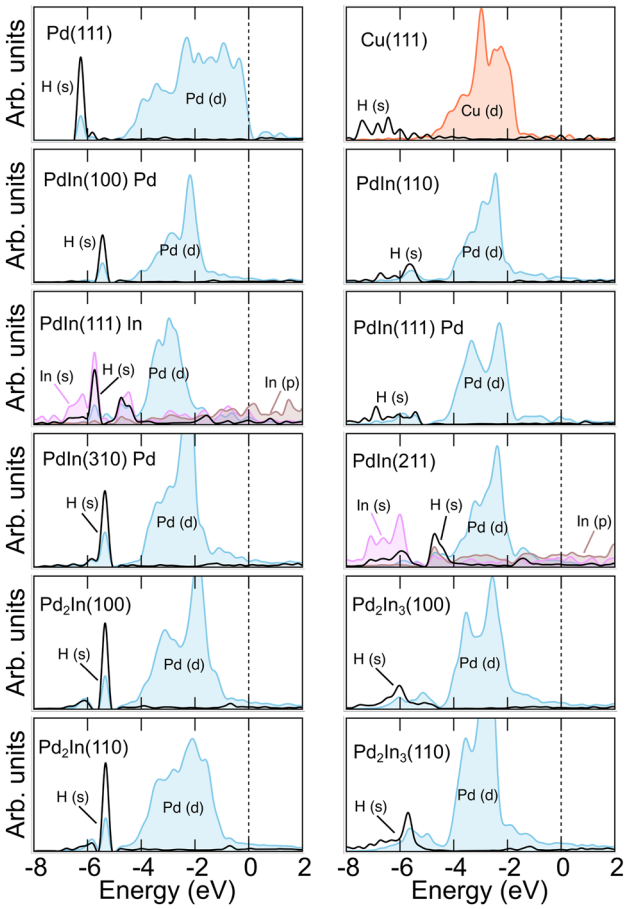

Fig. 3 Projected density of states (PDOS) for hydrogen (black line) adsorbed on Pd–In, Pd, and Cu surfaces. The surface PDOS includes atoms in direct contact with the adsorbed hydrogen atom. H(*s*), In(*s*), and In(*p*) states are scaled up by a factor of 5 compared to the Pd(*d*) and Cu(*d*) states to improve visibility. The In and Pd terminated surfaces are labelled with 'In' and 'Pd' after the surface indeces, respectively. The Fermi energy is shifted to 0 eV and indicated with a dashed vertical line

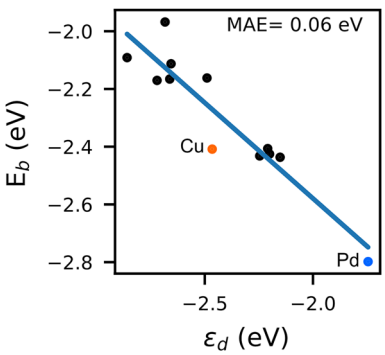

Fig. 4 Hydrogen binding energy (E_b) on the Pd, Cu, and Pd–In surfaces as a function of the *d*-band center (ϵ_d) of surface metal atoms. *d*-band center is calculated for the atoms on the clean metal surfaces that form the site which hydrogen adsorbs at

by In-Pd sites, and finally least favourably on In atop sites. The binding energy of hydrogen scales linearly with the projected *d*-band center of surface Pd atoms directly involved in bonding i.e. the closer the *d*-band center is positioned to the Fermi level, the stronger the binding energy. CO_2 hydrogenation is known to depend critically on the adsorption energy of hydrogen. The present work outlines how the composition and structure affect the hydrogen adsorption energy and can potentially be used to enhance the performance of PdIn-based CO_2 hydrogenation catalysts.

Acknowledgements This work was funded by the Knut and Alice Wallenberg Foundation (No: KAW 2015.0058) and the Swedish Research Council (2020-05191). The calculations were performed at NSC via a SNIC grant. The Competence Centre for Catalysis (KCK) is hosted by Chalmers University of Technology and financially supported by the Swedish Energy Agency and the member companies Johnson Matthey, Perstorp, Powercell, Preem, Scania CV, Umicore and Volvo Group.

Funding Open access funding provided by Chalmers University of Technology.

Data Availability All relaxed structures are available from the authors upon request.

Declarations

Conflict to declare There are no conflicts to declare.

References

1. Jiang X, Nie X, Guo X et al (2020) Recent advances in carbon dioxide hydrogenation to methanol via heterogeneous catalysis. Chem Rev 120(15):7984–8034. https://doi.org/10.1021/acs.chemrev.9b00723
2. De S, Dokania A, Ramirez A et al (2020) Advances in the design of heterogeneous catalysts and thermocatalytic processes for CO_2 utilization. ACS Catal 10(23):14,147-14,185. https://doi.org/10.1021/acscatal.0c04273
3. Zhang X, Zhang G, Song C et al (2021) Catalytic conversion of carbon dioxide to methanol: current status and future perspective. Front Energy Res 8(621):119. https://doi.org/10.3389/fenrg.2020.621119
4. Martin O, Martín AJ, Mondelli C et al (2016) Indium oxide as a superior catalyst for methanol synthesis by CO_2 hydrogenation. Angew Chem Int Ed 55(21):6261–6265. https://doi.org/10.1002/anie.201600943

5. Wang J, Zhang G, Zhu J et al (2021) CO_2 hydrogenation to methanol over In_2O_3-based catalysts: from mechanism to catalyst development. ACS Catal 11(3):1406–1423. https://doi.org/10.1021/acscatal.0c03665
6. Snider JL, Streibel V, Hubert MA et al (2019) Revealing the synergy between oxide and alloy phases on the performance of bimetallic In-Pd catalysts for CO_2 hydrogenation to methanol. ACS Catal 9(4):3399–3412. https://doi.org/10.1021/acscatal.8b04848
7. Frei MS, Mondelli C, García-Muelas R et al (2019) Atomic-scale engineering of indium oxide promotion by palladium for methanol production via CO_2 hydrogenation. Nat Commun 10(1):337. https://doi.org/10.1038/s41467-019-11349-9
8. García-Trenco A, Regoutz A, White ER et al (2018) PdIn intermetallic nanoparticles for the hydrogenation of CO_2 to methanol. Appl Catal B 220:9–18. https://doi.org/10.1016/j.apcatb.2017.07.069
9. Rui N, Wang Z, Sun K et al (2017) CO_2 hydrogenation to methanol over Pd/In_2O_3: effects of Pd and oxygen vacancy. Appl Catal B 218:488–497. https://doi.org/10.1016/j.apcatb.2017.06.069
10. Neumann M, Teschner D, Knop-Gericke A et al (2016) Controlled synthesis and catalytic properties of supported In-Pd intermetallic compounds. J Catal 340:49–59. https://doi.org/10.1016/j.jcat.2016.05.006
11. Wu Z, Wegener EC, Tseng HT et al (2016) Pd-In intermetallic alloy nanoparticles: highly selective ethane dehydrogenation catalysts. Catal Sci Technol 6:6965–6976. https://doi.org/10.1039/C6CY00491A
12. Penner S, Armbrüster M (2015) Formation of intermetallic compounds by reactive metal-support interaction: a frequently encountered phenomenon in catalysis. ChemCatChem 7(3):374–392. https://doi.org/10.1002/cctc.201402635
13. Fan J, Du H, Zhao Y et al (2020) Recent progress on rational design of bimetallic Pd based catalysts and their advanced catalysis. ACS Catal 10(22):13560–13583. https://doi.org/10.1021/acscatal.0c03280
14. Armbrüster M (2020) Intermetallic compounds in catalysis—a versatile class of materials meets interesting challenges. Sci Technol Adv Mater 21(1):303–322. https://doi.org/10.1080/14686996.2020.1758544
15. Hammer B, Norskov JK (1995) Why gold is the noblest of all the metals. Nature 376(6537). https://doi.org/10.1038/376238a0
16. Hammer B, Morikawa Y, Nørskov JK (1996) CO chemisorption at metal surfaces and overlayers. Phys Rev Lett 76:2141–2144. https://doi.org/10.1103/PhysRevLett.76.2141
17. Nilsson A, Pettersson LGM, Hammer B et al (2005) The electronic structure effect in heterogeneous catalysis. Catal Lett 100(3–4):111–114. https://doi.org/10.1007/s10562-004-3434-9
18. Hammer B, Nørskov J (2000) Theoretical surface science and catalysis-calculations and concepts. In: Impact of surface science on catalysis. Advanced Catalysis, vol 45, pp 71–129. Academic Press. https://doi.org/10.1016/S0360-0564(02)45013-4
19. Saini S, Stenlid JH, Abild-Pedersen F (2022) Electronic structure factors and the importance of adsorbate effects in chemisorption on surface alloys. NPJ Comput Mater. https://doi.org/10.1038/s41524-022-00846-z
20. Xin H, Linic S (2010) Communications: exceptions to the *d*-band model of chemisorption on metal surfaces: the dominant role of repulsion between adsorbate states and metal *d*-states. J Chem Phys 132(22):221101. https://doi.org/10.1063/1.3437609
21. Xin H, Vojvodic A, Voss J et al (2014) Effects of *d*-band shape on the surface reactivity of transition-metal alloys. Phys Rev B 89(115):114. https://doi.org/10.1103/PhysRevB.89.115114
22. Purdy SC, Seemakurthi RR, Mitchell GM et al (2020) Structural trends in the dehydrogenation selectivity of palladium alloys. Chem Sci 11:5066–5081. https://doi.org/10.1039/D0SC00875C
23. Armbrüster M, Kovnir K, Behrens M et al (2010) Pd-Ga intermetallic compounds as highly selective semihydrogenation catalysts. J Am Chem Soc 132(42):14745–14747. https://doi.org/10.1021/ja106568t
24. Wencka M, Hahne M, Kocjan A et al (2014) Physical properties of the InPd intermetallic catalyst. Intermetallics 55:56–65. https://doi.org/10.1016/j.intermet.2014.07.007
25. Posada-Borbón A, Grönbeck H (2021) A first-principles-based microkinetic study of CO_2 reduction to CH_3OH over In_2O_3(110). ACS Catal 11(15):9996–10006. https://doi.org/10.1021/acscatal.1c01707
26. Kauppinen M, Posada-Borbón A, Grönbeck H (2022) Methanol synthesis over PdIn, In_2O_3, and CuZn from first-principles microkinetics: Similarities and differences. J Phys Chem C 126(36):15235–15246. https://doi.org/10.1021/acs.jpcc.2c05715
27. McGuirk GM, Ledieu J, Gaudry E et al (2014) Surface structures of In-Pd intermetallic compounds. i. experimental study of In thin films on Pd(111) and alloy formation. J Chem Phys 141(8):084702. https://doi.org/10.1063/1.4892408
28. Gaudry E, McGuirk GM, Ledieu J et al (2014) Surface structures of In-Pd intermetallic compounds. ii. a theoretical study. J Chem Phys 141(8):084703. https://doi.org/10.1063/1.4892409
29. Rameshan C, Lorenz H, Armbrüster M et al (2018) Impregnated and co-precipitated $Pd\text{-}Ga_2O_3$, $Pd\text{-}In_2O_3$ and $Pd\text{-}Ga_2O_3\text{-}In_2O_3$ catalysts: Influence of the microstructure on the CO_2 selectivity in methanol steam reforming. Catal Lett 148(10):3062–3071. https://doi.org/10.1007/s10562-018-2491-4
30. Kresse G, Hafner J (1993) Ab initio molecular dynamics for liquid metals. Phys Rev B 47(1):558–561. https://doi.org/10.1103/PhysRevB.47.558
31. Kresse G, Hafner J (1994) Ab initio molecular-dynamics simulation of the liquid-metalamorphous-semiconductor transition in germanium. Phys Rev B 49(20):14251–14269. https://doi.org/10.1103/PhysRevB.49.14251
32. Kresse G, Furthmüller J (1996) Efficient iterative schemes for ab initio total-energy calculations using a plane-wave basis set. Phys Rev B 54(16):169
33. Kresse G, Furthmüller J (1996) Efficiency of ab-initio total energy calculations for metals and semiconductors using a plane-wave basis set. Comput Mater Sci 6:15–50
34. Kresse G, Joubert D (1999) From ultrasoft pseudopotentials to the projector augmented-wave method. Phys Rev B 59(3):1758–1775. https://doi.org/10.1103/PhysRevB.59.1758
35. Wellendorff J, Lundgaard KT, Møgelhøj A et al (2012) Density functionals for surface science: exchange-correlation model development with Bayesian error estimation. Phys Rev B 85(235):149. https://doi.org/10.1103/PhysRevB.85.235149
36. Avelar J, Bruix A, Garza J et al (2019) Van der Waals exchange-correlation functionals over bulk and surface properties of transition metals. J Phys Condens Matter 31(31):315501. https://doi.org/10.1088/1361-648x/ab18ea
37. Flandorfer H (2002) Phase relationships in the In-rich part of the In-Pd system. J Alloys Compd 336(1):176–180. https://doi.org/10.1016/S0925-8388(01)01859-X
38. Handbook CRC (2007) CRC handbook of chemistry and physics, 88th edn. CRC Press, Boca Raton
39. Fort D, Harris I (1975) The physical properties of some palladium alloy hydrogen diffusion membrane material. J Less-Common Met 41(2):313–327. https://doi.org/10.1016/0022-5088(75)90037-5
40. Kohlmanna H, Ritter C (2007) Refinement of the crystal structures of palladium-rich In-Pd compounds by X-ray and neutron powder diffraction. Z Naturforsch B 62(7):929–934. https://doi.org/10.1515/znb-2007-0709
41. Harris I, Norman M, Bryant A (1968) A study of some palladium-indium, platinum-indium and platinum-tin alloys. J Less-Common

Met 16(4):427–440. https://doi.org/10.1016/0022-5088(68)90141-0
42. Dewaele A, Loubeyre P, Mezouar M (2004) Equations of state of six metals above 94 GPa. Phys Rev B 70(094):112. https://doi.org/10.1103/PhysRevB.70.094112
43. Chen L, Medlin JW, Grönbeck H (2021) On the reaction mechanism of direct H_2O_2 formation over Pd catalysts. ACS Catal 11(5):2735–2745. https://doi.org/10.1021/acscatal.0c05548
44. Tang W, Sanville E, Henkelman G (2009) A grid-based Bader analysis algorithm without lattice bias. J Phys Condens Mater 21(8):084204. https://doi.org/10.1088/0953-8984/21/8/084204
45. Henkelman G, Arnaldsson A, Jónsson H (2006) A fast and robust algorithm for Bader decomposition of charge density. Comput Mater Sci 36(3):354–360. https://doi.org/10.1016/j.commatsci.2005.04.010
46. Yu M, Trinkle DR (2011) Accurate and efficient algorithm for Bader charge integration. J Chem Phys 134(6):064111. https://doi.org/10.1063/1.3553716
47. Sanville E, Kenny SD, Smith R et al (2007) Improved grid-based algorithm for Bader charge allocation. J Comput Chem 28(5):899–908. https://doi.org/10.1002/jcc.20575
48. Pang Tsai A, Kameoka S, Ishii Y (2004) PdZn=Cu: can an intermetallic compound replace an element? J Phys Soc Jpn 73(12):3270–3273. https://doi.org/10.1143/JPSJ.73.3270
49. Boer F, Boom R, Mattens W et al (1988) Cohesion in metals: transition metal alloys. Cohesion and structure, North-Holland. https://books.google.se/books?id=ZpdTAAAAMAAJ
50. Herron JA, Tonelli S, Mavrikakis M (2012) Atomic and molecular adsorption on Pd(111). Surf Sci 606(21):1670–1679. https://doi.org/10.1016/j.susc.2012.07.003
51. Grabow LC, Mavrikakis M (2011) Mechanism of methanol synthesis on Cu through CO_2 and CO hydrogenation. ACS Catal 1(4):365–384. https://doi.org/10.1021/cs200055d